Asian Journal of Social Science and Management Technology
ISSN: 2313-7410
Volume 6, Issue 4, July-August, 2024
Available at www.ajssmt.com

Adaptive Overcurrent Communication-Based Protection Scheme in Smart Distribution Systems in the Hybrid Grids

Amin Dindar

(Electric Power Engineers/ Austin, TX, USA)

ABSTRACT : One problem associated with the integration of renewable energy-based (RE-based) distributed generation (DG) is the malfunctions of protective devices within electric power distribution networks (EPDNs) as a result of generation intermittencies of these resources that cause a varying power injection to the EPDNs. To remedy this problem and as the objective of this study, a communication-assisted adaptive overcurrent protection coordination scheme (AOPCS) within a smart EPDN in the presence of wind and solar photovoltaic power generation is developed. Based on the AOPCS, the output power of DG units is distributed into several intervals based on a maximum acceptable error in the operating time of the relays. Then, the possible operating modes of the EPDN are determined, and for each possible mode of operation, the overcurrent relay setting parameters are calculated offline, while based on online monitoring of the EPDN, the operating mode is detected, and the relevant setting parameters are loaded into the relays. The obtained results indicate that AOPCS provides faster fault isolations without any malfunctions and nonselective operations of protective relays and much lower load curtailment as compared to the conventional overcurrent protection coordination scheme (COPCS).

Keywords - Overcurrent protection, wind power, photovoltaic system, distribution system protection, distributed generation.

---

1. NOMENCLATURE

1.1. Parameters and Constants

R_{cb}	Crowbar resistor (Ω)
CTI	Coordination time interval (s)
N_{DG}	Total number of DG units within the EPDN

1.2. Functions and variables

N_{OM}	Total number of possible operating modes of the EPDN
$N_{Int\,i}$	Total number of power intervals of i^{th} DG
PS	Power step (MW)
t	Operating time of relay (s)
TMS	Time multiplier setting of relay (s) turbine connection (V)
I_f	Fault current flowing through relay (A) interval for the next day
I_s	Pickup current of relay (A)

U Minimum line-to-line voltage at the point of DG units interconnection (p.u.)

t_D Disconnection time of DG units due to the LVRT requirement (s)

1.3. Acronyms

AOPCS Adaptive overcurrent protection coordination Scheme

COPCS Conventional overcurrent protection coordination scheme

DG Distributed generation

DFIG Doubly-fed induction generator

DOCR Directional overcurrent relay

EPDN Electric power distribution network

LVRT Low voltage ride-through

OC Overcurrent

PV Photovoltaic

RE Renewable energy

SI Standard inverse

2. Introduction

Recently, due to environmental concerns, renewable energy (RE) generation has gained a considerable penetration level within electric power distribution networks (EPDNs) to provide sustainable energy for the future [1] [2]. The integration of RE-based distributed generation (DG) with EPDNs introduces many benefits, such as a reduction in load curtailment duration due to main supply outages, voltage regulation, effective active and reactive power management, transmission and distribution loss reduction, and efficient and optimum operation of EPDN [3]. However, the integration of RE-based DG units with EPDNs causes a higher level of complexity in the operation, control, management, and protection of EPDNs [4-6]. The effects of DG units on the protection of EPDNs and the related issues are widely evaluated in the literature [5-8]. Some of these effects can be summarized as follows.

First, in the presence of DG units, depending on the size and location of DG units and the amount of load, power flow in some parts of the EPDN may be bi-directional. Therefore, the conventional protection schemes that only consider uni-directional power flow may be inadequate [9]. Second, normal and short-circuit current levels in many branches may vary, and this may result in delayed or nonselective operations of overcurrent (OC) relays [3]. Moreover, protection blinding, false tripping, and problems with recloser operation are other issues associated with the integration of DG units with EPDNs [5, 8]. To cope with such problems, adaptive protection schemes are introduced in the literature [10]. Generally, adaptive protection algorithms dynamically modify the setting parameters of protective devices in response to any change in the operating mode of EPDNs and provide an optimum operation, i.e., fast and correct operation of protective devices considering coordination constraints [10]. In [11], adaptive current protection in EPDNs, including DG units, was proposed. The work in [12] suggested an adaptive OC protection scheme in EPDNs with DG units and concluded considerable improvements against conventional protection schemes. An adaptive OC protection scheme in EPDNs, including wind power generations, was proposed in [9], which examines the connection/disconnection status of DG units to adaptively modify the setting parameters of directional OC relays (DOCRs). The results of that study show significant improvements in the operation of DOCRs compared to a conventional protection scheme. The work in [13] proposed a fuse-relay adaptive protection scheme that groups identical inverse time OC settings of relays and logic gates of relay breakers to achieve better selectivity, reliability, and faster fault isolations. An adaptive protection coordination scheme for power networks in the presence of DG units was proposed in [14], which optimizes the setting parameters of relays and maintains coordination between OC relays and distance relays. In [15], an adaptive optimization strategy was proposed to optimize the operation of OC relays in a microgrid under different operating modes. In [16], an algorithm was proposed to adaptively change the settings of differential relays according to the power injection (wind speed) of wind turbines to protect the transformer that connects the wind turbine to the grid. Adaptive and non-adaptive backup OC protection on fuse feeders

with different ratings were compared in [17], and the results indicated that the adaptive coordination of OC relay with fuse feeders provides faster fault isolations with better selectivity. In [18], it was shown that by using sequence components, the faults can be identified without using communication-assisted protection in a power system with penetration of photovoltaic (PV)-based DGs. In [19], authors proposed a novel approach to dynamically reconfigure protective devices used to implement advanced fault location, isolation, and service restoration solutions. As the objective of this study, a communication-assisted adaptive OC protection coordination scheme (AOPCS) within a smart EPDN in the presence of wind and solar PV power generations is developed. The reference [31] proposed using advanced machine learning algorithms, including random forests, XGBoost, LightGBM, CatBoost, and MLP-ANNs, to forecast solar irradiance for optimizing PV systems in smart grids. Bayesian optimization was used for hyperparameter tuning. The results showed that feature selection improves MLP-ANN performance, with random forests outperforming the other algorithms. Finally, [32] and [33] introduced optimization frameworks integrating ML tools such as MNL, which could be used in energy demand forecasting and pricing.

In contrast to other studies, accurate models and low voltage ride-through (LVRT) requirements for DG units are taken into account in this study. The output power of DG units is distributed into several intervals considering a maximum acceptable error in the operating time of the relays, and the operating modes of the EPDN are determined based on these intervals. The setting parameters of DOCRs are calculated offline, and based on online monitoring of the EPDN, the operating mode is detected. Then, these setting parameters are loaded into the relays using communication infrastructures. In this study, the AOPCS loads the setting parameters of relays based on the operating mode of the EPDN, and the directional element of the DOCRs is responsible for detecting the direction of the fault current to provide a selective operation of the relays. In addition, three-phase faults are located in various locations, and the performance of AOPCS is compared with a conventional OC protection coordination scheme (COPCS). The remainder of this study is organized as follows: Section 2 provides the methodology of implementing the proposed AOPCS; in Section 3, test EPDN, DG units modeling, and related parameters, DOCRs coordination approach, and other simulation data are provided; results and discussion are provided in Section 4; and conclusions and future work suggestions are discussed in Section 5.

3. METHODOLOGY

The proposed AOPCS in smart EPDNs, including wind and PV power generations, is introduced in this section. The flowchart of the proposed AOPCS is shown in Fig 1. This scheme consists of both offline calculations and online monitoring of the EPDN for detecting the real-time operating mode. The steps of the AOPCS are as follows:

The offline calculations consist of the following:

Step 1: The algorithm starts with the input data of the EPDN, such as topology, lines, loads, and transformers parameters, the acceptable error in operating time of relays, and the data of DG units, including rated power, type, point of connection, and LVRT requirement.

Step 2: Using the output information of Step 1 as input data in this step, all possible operating modes of the EPDN and the corresponding setting parameters of relays for each operating mode are calculated. If the monitored output power of a DG unit is within an interval and is equal to or greater than the midpoint of that interval, the upper limit of the interval is considered as the output power of that DG unit. Otherwise the lower limit is considered as the output power of the DG unit. Afterward, the power flow and short circuit analyses are performed, and the setting parameters of all relays in all operating modes are calculated and saved in a lookup table.

Online operations consist of the following:

Step 3: By monitoring the EPDN, the real-time output power of all DG units is observed.

Step 4: Based on the results of Step 3, if there is any change in the operating mode of the EPDN, the output of

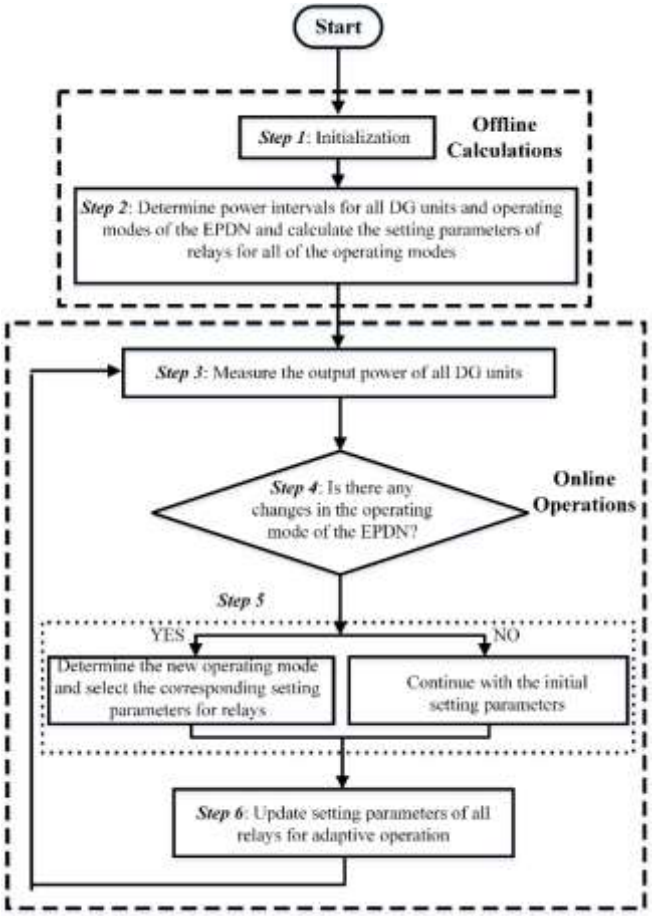

Fig. 1. Flowchart of the proposed AOPCS

this step is YES, otherwise NO.

Step 5: If the output of Step 4 is YES, which shows a change in the operating mode of the EPDN, the new operating mode is determined, and relevant setting parameters are selected from the lookup table. For NO in Step 4, the setting parameters of the relays are unchanged.

Step 6: The calculated setting parameters from Step 5 are sent to relays for adaptive protection. The algorithm then returns to Step 3, and this loop is repeated.

It should be mentioned that in Step 2, the following approach is adopted to distribute the output power of each DG unit into some intervals.

First, the operating time of all relays when all DG units are connected to the EPDN and generating their rated power (rated wind speed for wind turbines and standard irradiance and temperature for solar modules) for faults at different points of the EPDN are determined.

Second, the wind speed and solar irradiance are decreased discretely, and keeping the temperature in a constant value (the goal is to decrease the output power of solar PV units by only changing the irradiance) and the operating time of relays are calculated. Once the error in operating time of relays reaches a maximum acceptable error (MAE) value or a malfunction is observed, the output power of DG units is subtracted from their rated output power, and this value is called the power step (PS), and multiplied by two to obtain the length of power intervals for each DG unit.

Third, all the power intervals for all DG units are determined by building the intervals from the rated power to reach zero output power.

Finally, all intervals' first and end points are considered possible generation values of all DG units. The total number of possible operating modes is the multiplication of the number of considered possible output power of all DG units and is calculated as:

$$N_{OM} = \prod_{i=1}^{N_{DG}} (N_{Int,i} + 1) \qquad (1)$$

It is worthwhile to mention that in Step 4 of the AOPCS if the monitored power of DG units is equal to or greater

than the midpoint of an interval and lower than the end point of that interval, the output power is considered to be the end point of that interval. If it is between the first point and midpoint of an interval, the output power is determined to be the first point of that interval.

For determining the power intervals, all DG units are connected to the EPDN and are generating their rated power because, in this operating condition, DG units have the highest influence on the currents flowing through the EPDN branches and, therefore, on the operating time of all relays.

In addition, there is a trade-off between the number of intervals, which determines the number of operating modes, and the accuracy of the operating time of the relays. If the MAE is decreased, the number of power intervals and, therefore, the total number of operating modes will increase. Also, the AOPCS algorithm is embedded in a central processing unit, and all the data transfer and system monitoring operations are feasible in a smart EPDN. To show the effectiveness of the proposed AOPCS, a COPCS is also examined. In COPCS, all DG units are connected to the EPDN, and generate their rated power and the setting parameters of the relays are calculated once and do not change in response to changes in the EPDN operating mode. Moreover, in the proposed AOPCS, once the setting parameters are calculated, they can be used in the EPDN for each time interval and operating condition until the configuration or size and location of DG units within the EPDN are changed.

4. TEST NETWORK AND SIMULATION DATA

All the simulations in this study are carried out in MATLAB/Simulink environment, and modeling of each component in this environment is discussed in detail in the following sections. The distribution network used in [8] is considered as a test EPDN (Fig. 2) which is equipped with a central control unit and communication and monitoring infrastructures for the implementation of the AOPCS. In addition, three DG units, including two doubly-fed induction generator (DFIG) wind turbines with a rated output power of 1.5 MW and one solar PV unit with a rated output power of 1 MW, are connected to Buses 3, 5, and 6, respectively. This EPDN is connected to the power grid, which is modeled as a 50 kV line-to-line infinite bus with a rated frequency of 50 Hz. The relevant data for lines and loads is provided in [8].

1.4. Wind Power Generation Modeling

In this study, DFIG-based wind turbines, as the most common generator type for wind farms, are considered as wind power generation units [20]. For the purpose of adaptive protecton, a dynamic model for DFIG-based wind

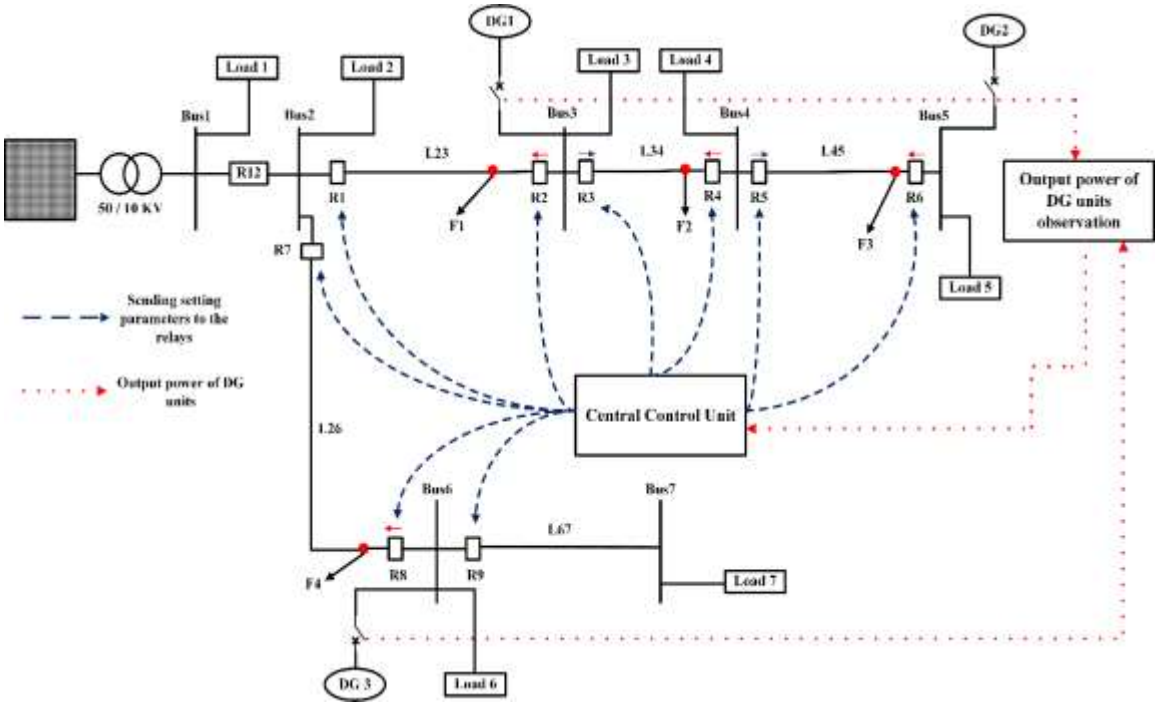

Fig. 2. Network diagram of the test EPDN used in this study [8]

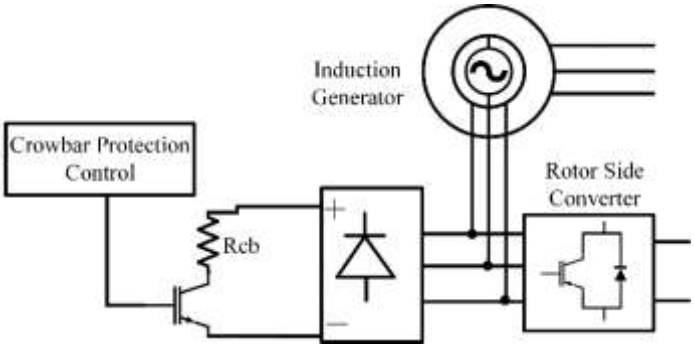

Fig. 3. Schematic diagram of crowbar protection [20]

turbines is required. Therefore, the proposed model in [21] with some modifications is used. This model is available in MATLAB/Simulink, named DFIG Detailed Model, and the modifications made are as follows:

- A crowbar resistor is added to the rotor circuit to protect the rotor and converters during the fault occurrence in the EPDN. A crowbar resistor shorts the circuit of the rotor during fault occurrences [20]. Also, the use of crowbar protection enables the DFIG to comply with the LVRT requirement defined in Grid Codes and to stay connected to the grid to generate power immediately after the fault clearance. The schematic of crowbar protection is shown in Fig. 3 [20], where the crowbar protection control unit fires the power switch when the rotor current becomes greater than a predefined value to short circuit the rotor with a crowbar resistor for reducing rotor current and protection of rotor and converters.

- LVRT, which is a Grid Code for wind power integration into power networks, is considered in this study shown in Fig 4 [22], where the vertical axis indicates the smallest line-to-line voltage in p.u. at the point of connection. According to this Grid Code, the wind power generation is allowed to disconnect from the grid only when the voltage profile falls into Area C.

Also, the relevant data for wind turbines are available on DFIG Detailed Model example in MATLAB/Simulink environment. In addition, the results from reference [23] are used to determine the value of the crowbar resistor. So, the value of the crowbar resistor is set to be 30 times greater than the rotor resistance; therefore, since the rotor resistance is 0.016 p.u., the crowbar resistor is determined to be 0.48 p.u. and in terms of ohm, it becomes 1.1232Ω (the rotor rated line-to-line voltage is 1975 V, and the generator rated apparent power is (1.5/0.9)×106 VA). Moreover, the threshold of rotor current at which the crowbar protection control unit activates its power switch is determined to be 1.5 p.u. [24].

1.5. Solar PV power Generation Modeling

This study uses a detailed model of a grid-connected PV array from Matlab/Simulink environment as a solar PV power generation model. In this model, the number of parallel strings is increased to 660 to obtain a 1

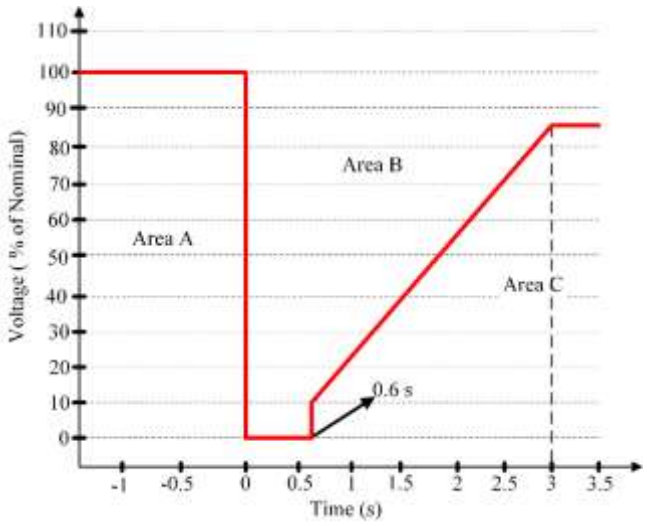

Fig. 4. LVRT requirement for wind and solar power generation [22]

MW solar PV power generation unit without changing the rated voltage of the strings. Also, the LVRT requirement shown in Fig. 4 is considered for the connection of this solar PV power generation unit [22]. In addition, the current injected by this unit is limited to 2 times its rated current [25].

1.6. DOCRs Coordination Approach

Since the DG units are connected to different points of the distribution system, the flow of power is bi-directional in some areas, and this depends on the location and generation capacity of DG units and also the amount of load in busbars; therefore, the use of DOCR relays in the distribution system for OC protection is unavoidable. In this study, as shown in Fig 2, DOCRs with different directions are embedded in each line to effectively trip the faulted area and maintain selectivity. It is worth mentioning that R1, R7, and R9 are OC relays because the current always flows through one direction, and there is no need to use a DOCR in these points. The directional element of DOCRs is implemented using the method presented in [26]. In addition, the standard inverse (SI) characteristic, which is defined by IEC 60255, is used for the OC characteristic of DOCRs. The operating time of SI relays can be calculated as:

$$t = \frac{TMS \times 0.14}{\left[\left(\frac{I_f}{I_s}\right)^{0.02} - 1\right]}, \qquad (2)$$

Where I_S is the pickup current of the relay, TMS is the time multiplier setting of the relay, and I_f is the fault current flowing through the relay. If the current is flowing in the forward direction and is greater than I_S, then after a time delay, which is calculated using Eq. (2), the relay sends the trip signal to the corresponding circuit breaker. In addition, the coordination is carried out using the procedure explained in [9].

5. RESULTS AND DISCUSSION

Changing wind turbines and solar PV unit parameters, i.e., wind speed, irradiance, and temperature results in changes in the setting parameters of relays in AOPCS. For instance, when the wind speed is equal to its rated value (15m/s) and the solar PV unit operates in standard test conditions (irradiance= 1000 $\frac{\text{w}}{\text{m}^2}$ and temperature= 250C), the pickup current of R2 and R8 are 225.7A and 75.1A, respectively. Under these conditions, when a three-phase fault is applied in point F1, the fault current flowing through R2 and R8 at 0.1s after the fault occurrence is 299.8A and 53.2A, respectively. However, when the wind speed is equal to 10m/s and the irradiance is 500 $\frac{\text{w}}{\text{m}^2}$ with a temperature of 250C, the pickup current of R2 and R8 are 137.2A and 35.4A, respectively. Also, when a three-phase fault is applied in point F1, the fault current flowing through R2 and R8 at 0.1s after the fault occurrence is 305.2A and 33.2A, respectively. According to this example, changes in the parameters of wind and solar PV units result in changes in relay setting parameters and fault currents, which are considered in AOPCS. However, in COPCS, these variations are not considered [27].In this study, it is assumed that the test EPDN is located in Adelaide, Australia, and the AOPCS is tested for a typical day whose wind speed and temperature data are provided in Table I [28, 29], and its solar irradiance data is shown in Fig. 5 [30].

TABLE I: The arrangement of channels wind speed and temperature of a typically day in Adelaide, Austrailia [27, 28].

Hour	Wind speed (m/s)	Temperature (°C)	Hour	Wind speed (m/s)	Temperature (°C)	Hour	Wind speed (m/s)	Temperature (°C)
1	3	19	9	1.5	22	17	6.5	30
2	3	19	10	2	23	18	7	29
3	2.5	18	11	4	28	19	8	22
4	2	18	12	4.5	28	20	9.5	22
5	1.5	17	13	5	28	21	7	21
6	2	17	14	6	28	22	6	21
7	2	17	15	6.5	29	23	2	20
8	1.5	21	16	6	30	24	1	19

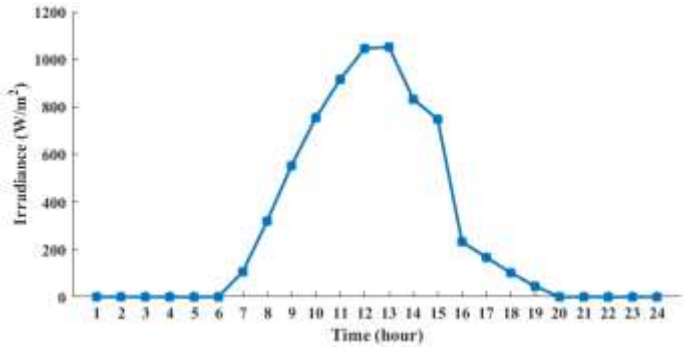

Fig. 5. Solar irradiance in a typical day in Adelaide, Australia [29]

Considering the DG units modeling approach, the short circuit current injection by DG units when a three-phase fault occurs at point F2 at hour 14 is shown in Fig. 6. According to the AOPCS and by considering the MAE of 20%, the PS for wind turbines and the solar PV unit is determined to be 0.1 MW and 0.05 MW, respectively. Therefore, the power intervals for wind turbines are (1.3,1.5), (1.1,1.3), (0.9,1.1), (0.7,0.9), (0.5,0.7), (0.3,0.5), (0.1,0.3), (0,0.1), and for the solar PV unit, the power intervals are (0.9,1), (0.8,0.9), (0.7,0.8), (0.6,0.7), (0.5,0.6), (0.4,0.5), (0.3,0.4), (0.2,0.3), (0.1,0.2), and (0,0.1). Based on the calculated power intervals, the total number of possible operating modes of the EPDN is $N_{OM} = 9 \times 9 \times 11 = 891$. Also, in this section, two cases are considered. First, it is assumed that the DG units do not disconnect from the EPDN due to the LVRT requirement (Case 1). Second, DG units are disconnected from the EPDN when the voltage profile of the point of connection falls into area C of Fig. 4 (Case 2). Note that AOPCS can be employed in an EPDN for any time and any mode of operation. In other words, once the setting parameters are determined, they can be used until DG units' configuration, or size and location are altered.

1.7. Case 1

The relay operating times for some sample hours and with three-phase faults in various locations when employing COPCS and AOPCS are provided in Table 2 and Table 3, respectively. Comparing these two tables shows that the relay operating times for these sample hours in AOPCS are much shorter than those of COPCS. The sum of all operating times of primary and backup relays in 24 hours with faults at points F1, F2, F3, and F4 is 124.3268s for COPCS and 95.5083s for AOPCS. Based on the obtained results, AOPCS provides faster fault isolations as compared to COPCS. In addition, in some hours and fault points, a violation of the CTI criterion is observed when employing COPCS, which is provided in Table 4. In this case, load curtailment due to the fault occurring within the EPDN in both COPCS and AOPCS is the same because DG units are not disconnected from the EPDN due to the LVRT requirement.

1.8. Case 2

Based on Fig. 4, when the voltage at the point of connection in p.u. is lower than 0.1, the disconnection time of DG units is 0.6s, and when it is greater than 0.85, the DG unit stays connected to the EPDN and its disconnection

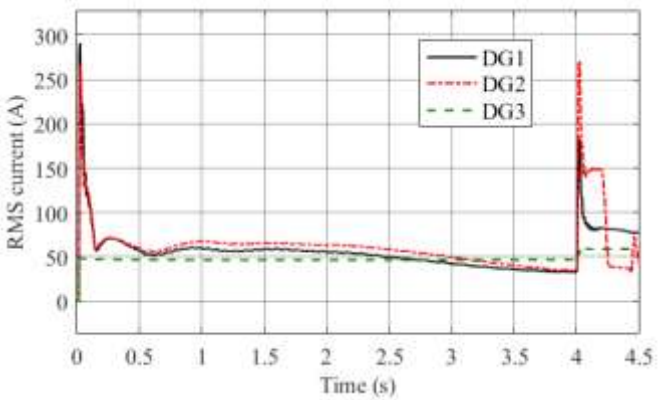

Fig. 6. Short circuit current of DG units with a three-phase fault at point F2 at hour 14

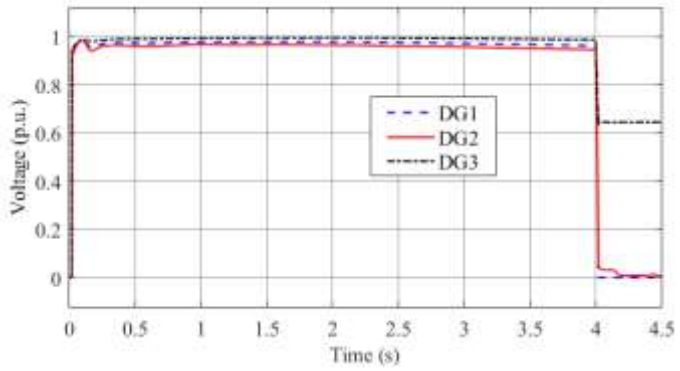

Fig. 7. Voltage profile for DG units for hour 15 with three-phase fault at point F1

time is infinite. For the values of voltage between 0.1 p.u. and 0.85 p.u., the relationship between the time delay and the voltage is linear. Therefore, the following function can be defined to calculate the disconnection time of the DG units.

In each mode of operation, when a fault occurs within the EPDN, the disconnection time of the DG units is calculated using Eq. (3).

$$t_D = \begin{cases} 0.6; U < 0.1 \\ 3.2U + 0.28; 0.1 \leq U < 0.85. \\ \infty; U \geq 0.85 \end{cases} \quad (3)$$

If the calculated t_D for a DG unit is lower than the operating time of a relay that sends the trip signal to the circuit breaker through which the short circuit current of that DG unit is feeding the fault, the relevant DG unit is disconnected from the grid and has no contribution to the fault and therefore, that circuit breaker does not operate. But if the opposite holds true, the circuit breaker operates, and the DG unit does not disconnect from the EPDN. For instance, in hour 15 and when a three-phase fault is applied at point F1 at t=4s, the value of V for all DG units is shown in Fig. 7. Based on Fig. 7 and Eq. (3), the disconnection time for DG1, DG2, and DG3 are determined as 0.6s, 0.6s, and 2.36s, respectively. In AOPCS, the operating time of R2 and R4 when a three-phase fault occurs at point F1 is 0.2768s and 0.5769s, respectively. Therefore, the fault is being cleared faster than the disconnection of DG units, and all DG units stay connected to the EPDN. However, in COPCS, the operating time of R2 and R4 is 0.9966s and 1.2642s and therefore, DG1 and DG2 are disconnected from the EPDN, and only R1 operates. As a result, since the operating time of relays is high in COPCS, DG units become disconnected more, and they cannot supply the load immediately after the fault clearance. So, more load curtailments are exercised in the EPDN when employing COPCS. For example, in the mentioned example, the amount of active load curtailment in COPCS due to fault occurrence in point F1 is 4 MW, and in AOPCS, it is 2.56 MW. The total amount of active load curtailment in 24 hours and due to the fault occurrence in specified points in Fig. 2, i.e, points F1, F2, F3, and F4 (considering the proper operation of main relays) in COPCS and AOPCS is 216 MW and 193.59 MW, respectively. This amount of reduction in load curtailment is a result of faster fault isolation in AOPCS as compared to COPCS. Therefore, the EPDN reliability is improved when employing AOPCS in comparison to the

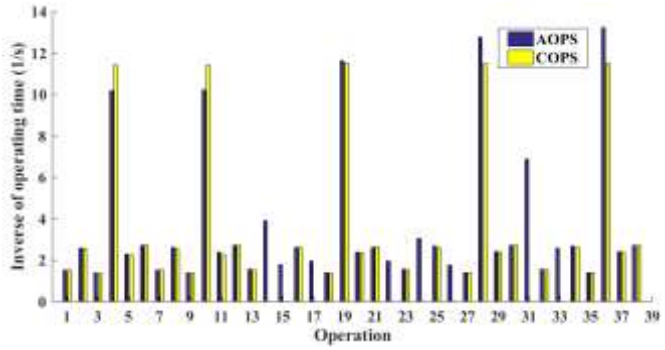

Fig. 8. Inverse of operating times in Case 2

COPCS. For a better representation, the inverse of relay operating times for some sample hours and with three-phase faults in various locations when employing both COPCS and AOPCS, just like Case 1, are provided in Fig. 8. Since Fig. 8 shows the inverse of operating times, the higher values in this figure indicate a shorter operating time. In Fig. 8, each operation in the horizontal axis shows a relay operation when a three-phase fault is applied in one of the F1, F2, F3, and F4 points at a specific hour, just like in Case 1. For example, the first operation in Fig. 8 is the operation of relay R1 at hours 1-6, 23, and 24 when a three-phase fault is applied at point F1. The other operations are related to main and backup relays operation when three-phase faults are applied in points and hours indicated in Table 2 as in Case 1. It is noted that in some operations in Fig. 8, the values in COPCS is zero; this indicates that the corresponding relays do not operate. As it is shown in Fig. 8, in almost all operations, the operating times in AOPCS are shorter than those of COPCS. In this case, the sum of all operating times of main and backup relays, which operate in both COPCS and AOPCS in 24 hours with three-phase faults at points F1, F2, F3, and F4 is 69.4748s for COPCS and 66.0173s for AOPCS. In addition, since the operating time of relays in COPCS is higher than those of AOPCS, in all conditions, DG units are disconnected before the operation of the relay, and therefore, the reverse direction relays (R2, R4, R6, R8) do not operate.

In addition, in both Case 1 and Case 2, when the COPCS is employed, the normal current flowing through R1 and R7 is higher than their pickup current. Therefore, R1 and R7 send the trip signal wrongly, making the EPDN disconnected from the primary grid. For example, in hour 17, in the normal operating condition of the EPDN, the current flowing through R1 and R7 is 165.9A and 46.4A, respectively, which results in the operation of R1 at t=5.7306s and R7 at t=1.2165s. As a result, the EPDN becomes disconnected from the primary grid. The difference between the total load and the total power generated by DG units is the amount of load curtailed without any fault occurring within the EPDN. The amount of load curtailments in COPCS in the normal operating mode of the EPDN is provided in Fig. 9. According to Fig. 9, the amount of load curtailment in each hour depends on the amount of power generated by DG units. For instance, in hour 14, since the total power generated by DG units is the most, the amount of curtailed load is the lowest value in all hours. However, the employment of AOPCS prevents such load curtailments. Since the value of the lost load is significant in almost all EPDNs, these

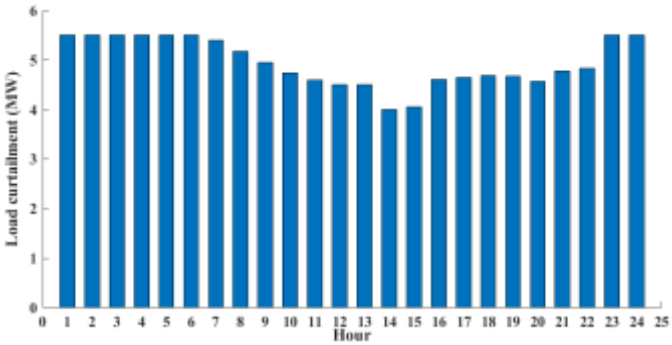

Fig. 9. Active load curtailment in COPCS in normal operating mode of the EPDN

load curtailments are unacceptable within an EPDN and cause a considerable cost for the distribution company. The employment of the proposed AOPCS in this study can prevent such unwanted load curtailments and provide a reliable protection scheme for EPDNs with high penetration levels of RE-based DG units. It is noted that implementing the proposed AOPCS requires a smart EPDN with at least a local area network for communicating the relays setting parameters between the central control unit and the relays and monitoring DG units output power within the EPDN. Also, the reliable and accurate operation of the communication network plays a vital role in the favourable performance of the AOPCS. In addition, a data storage capacity at the central control unit is required for saving all setting parameters related to each mode of operation.

6. Conclusions and Future Work Suggestion

In this study, a communication-assisted AOPCS is proposed for the protection of EPDNs, including DFIG wind turbines and solar PV panels as DG units. The proposed scheme is based on distributing the output power of DG units into several intervals and then determining the setting parameters of DOCRs for all possible operating

modes of the EPDN. The proposed scheme is examined for a sample EPDN including three DG units and by applying three-phase faults in various locations. Moreover, the results are provided with and without considering the disconnection of DG units due to the LVRT requirement.

According to the obtained results, the AOPCS provides selective and fast fault isolations as compared to the COPCS. Moreover, mal-operations, non-selective actions, and unnecessary load curtailments in COPCS are avoided by the AOPCS. Based on the simulation results, it is also observed that by implementing AOPCS, a total reduction of 23.18% in one case and 4.98% in the other case in operating times is achieved for the test EPDN. In addition, when the DG units are disconnected from the EPDN due to the LVRT requirement, the effectiveness of the AOPCS is decreased while providing better protection performance as compared to the COPCS.

For future extension of this study, implementing adaptive protection schemes considering various scenarios with their probability of occurrence for output power of RE-based DG units is of interest. Also, implementing the AOPCS in an EPDN considering the optimal allocation of DG resources in terms of DG units rated power and point of connection and also quantifying reliability improvements are recommended.

Appendix

TABLE II: Operating times in COPCS in Case 1

Hour	Fault point	Main relays operating time (s)	Backup relays operating time (s)	Time difference between main and backup relays (s)
1-6, 23, 24	F1	R1=0.6468	……	……
	F2	R3=0.3901	R1=0.7352	R1-R3=0.3451
	F3	R5=0.0874	R3=0.4379	R3-R5=0.3505
	F4	R7=0.3662	……	……
12,13	F1	R1=0.6467	……	……
	F2	R3=0.3898	R1=0.7357	R1-R3=0.3459
	F3	R5=0.0873	R3=0.4377	R3-R5=0.3504
	F4	R7=0.3662 R8=0.7555	……	……
14	F1	R1=0.645 R2=1.0359	R4=1.3125	R4-R2=0.2766
	F2	R3=0.3809 R4=0.9811	R1=0.7229 R6=1.3507	R1-R3=0.342 R6-R4=0.3696
	F3	R5=0.0869 R6=1.1657	R3=0.4229	R3-R5=0.336
	F4	R7=0.3778 R8=0.7555	……	……
19	F1	R1=0.6454 R2=1.0418	R4=1.3342	R4-R2=0.2924
	F2	R3=0.3809 R4=0.9851	R1=0.7113 R6=1.37	R1-R3=0.3304 R6-R4=0.3849
	F3	R5=0.0869 R6=1.1666	R3=0.418	R3-R5=0.3311
	F4	R7=0.3654 R8=0.7555	……	……
20	F1	R1=0.6457 R2=1.1149	R4=1.4232	R4-R2=0.3083
	F2	R3=0.3812 R4=1.0293	R1=0.7094 R6=1.4845	R1-R3=0.3282 R6-R4=0.4552
	F3	R5=0.0869 R6=1.2602	R3=0.4183	R3-R5=0.3314

	F4	R7=0.3655	……	……

TABLE Ⅲ: Operating times in AOPCS in Case 1

Hour	Fault point	Main relays operating time (s)	Backup relays operating time (s)	Time difference between main and backup relays (s)
1-6, 23, 24	F1	R1=0.6457	……	……
	F2	R3=0.3835	R1=0.708	R1-R3=0.3245
	F3	R5=0.0981	R3=0.4379	R3-R5=0.3398
	F4	R7=0.3654	……	……
12,13	F1	R1=0.6446	……	……
	F2	R3=0.3831	R1=0.7072	R1-R3=0.3459
	F3	R5=0.098	R3=0.4204	R3-R5=0.3224
	F4	R7=0.3655 R8=0.7555	……	……
14	F1	R1=0.6405 R2=0.255	R4=0.555	R4-R2=0.3
	F2	R3=0.3793 R4=0.5113	R1=0.709 R6=0.8114	R1-R3=0.3297 R6-R4=0.3001
	F3	R5=0.0858 R6=0.7825	R3=0.4182	R3-R5=0.3324
	F4	R7=0.3798 R8=0.5133	……	……
19	F1	R1=0.6333 R2=0.3268	R4=0.6269	R4-R2=0.3001
	F2	R3=0.3731 R4=0.5649	R1=0.7093 R6=0.8651	R1-R3=0.3362 R6-R4=0.3002
	F3	R5=0.0783 R6=0.824	R3=0.4146	R3-R5=0.3363
	F4	R7=0.3654 R8=0.1451	……	……
20	F1	R1=0.6318 R2=0.3876	R4=0.6878	R4-R2=0.3002
	F2	R3=0.3712 R4=0.6081	R1=0.7067 R6=0.9085	R1-R3=0.3355 R6-R4=0.3004
	F3	R5=0.0757 R6=0.859	R3=0.4113	R3-R5=0.3356
	F4	R7=0.3657	……	……

TABLE Ⅳ: Violations of CTI criterion in COPCS in Case 1

Hour	Fault point	Main relay operating time (s)	Backup relay operating time (s)	Time difference between main and backup relays (s)
14	F1	R2=1.0359	R4=1.3125	0.2766
16	F1	R2=1.0379	R4=1.3152	0.2773
17	F1	R2=0.9975	R4=1.2666	0.2691
18	F1	R2=1.002	R4=1.2891	0.2871
19	F1	R2=1.0418	R4=1.3342	0.2942
21	F1	R2=0.9948	R4=1.2765	0.2817
22	F1	R2=1.055	R4=1.3397	0.2847

7. REFERENCES

[1] R. Nematirad and A. Pahwa, "Solar Radiation Forecasting Using Artificial Neural Networks Considering Feature Selection," 2022 IEEE Kansas Power and Energy Conference (KPEC), Manhattan, KS, USA, 2022, pp. 1-4, doi: 10.1109/KPEC54747.2022.9814765.

[2] R. Nematirad, M. M. Ardehali, A. Khorsandi, and A. Mahmoudian, "Optimization of Residential Demand Response Program Cost with Consideration for Occupants Thermal Comfort and Privacy," in IEEE Access, vol. 12, pp. 15194-15207, 2024, doi: 10.1109/ACCESS.2024.3358404.

[3] S. Ourang, "Water resources management optimization and development of sustainable agriculture, case study: Pakdasht plain," J Agric Sci Bot 2017; 1 1-5. 2 J Agric Sci Bot 2017 Vol. 1 Issue, vol. 1, no. 41700, p. 74165, 2017, doi: 10.35841/2591-7897.1.1.25-29.

[4] Z. Wang, J. Wang, and C. Chen, "A three-phase microgrid restoration model considering unbalanced operation of distributed generation," IEEE Trans. Smart Grid, vol. 9, no. 4, pp. 3594–3604, 2016, doi: 10.1109/TSG.2016.2621412.

[5] Nematirad, R.; Pahwa, A.; Natarajan, B. A Novel Statistical Framework for Optimal Sizing of Grid-Connected Photovoltaic–Battery Systems for Peak Demand Reduction to Flatten Daily Load Profiles. Solar 2024, 4, 179-208. https://doi.org/10.3390/solar4010008.

[6] R. Nematirad, M. Behrang and A. Pahwa, "Acoustic-Based Online Monitoring of Cooling Fan Malfunction in Air-Forced Transformers Using Learning Techniques," in IEEE Access, vol. 12, pp. 26384-26400, 2024, doi: 10.1109/ACCESS.2024.3366807.

[7] W. Kou and D. Wei, "Fault ride through strategy of inverter-interfaced microgrids embedded in distributed network considering fault current management," Sustain. Energy, Grids Networks, vol. 15, pp. 43–52, 2018, doi: 10.1016/j.segan.2017.12.003.

[8] V. A. Papaspiliotopoulos, G. N. Korres, and N. D. Hatziargyriou, "Adverse impact of distributed generation on protection of the Hellenic MV network–recommendations for protection scheme upgrade," CIRED-Open Access Proc. J., vol. 2017, no. 1, pp. 934–938, 2017, doi: 10.1049/oap-cired.2017.1160.

[9] B. P. Bhattarai, B. Bak-Jensen, S. Chaudhary, and J. R. Pillai, "An adaptive overcurrent protection in smart distribution grid," in 2015 IEEE Eindhoven PowerTech, 2015, pp. 1–6, doi: 10.1109/PTC.2015.7232310.

[10] Y. Ates, M. Uzunoglu, A. Karakas, A. R. Boynuegri, A. Nadar, and B. Dag, "Implementation of adaptive relay coordination in distribution systems including distributed generation," J. Clean. Prod., vol. 112, pp. 2697–2705, 2016, doi: 10.1016/j.jclepro.2015.10.066.

[11] L. Che, M. E. Khodayar, and M. Shahidehpour, "Adaptive Protection System for Microgrids: Protection practices of a functional microgrid system.," IEEE Electrif. Mag., vol. 2, no. 1, pp. 66–80, 2014, doi: 10.1109/MELE.2013.2297031.

[12] J. Ma, X. Wang, Y. Zhang, Q. Yang, and A. G. Phadke, "A novel adaptive current protection scheme for distribution systems with distributed generation," Int. J. Electr. Power Energy Syst., vol. 43, no. 1, pp. 1460–1466, 2012, doi: 10.1016/j.ijepes.2012.07.024.

[13] F. Coffele, C. Booth, and A. Dyśko, "An adaptive overcurrent protection scheme for distribution networks," IEEE Trans. Power Deliv., vol. 30, no. 2, pp. 561–568, 2014, doi: 10.1109/TPWRD.2013.2294879.

[14] E. C. Piesciorovsky and N. N. Schulz, "Fuse relay adaptive overcurrent protection scheme for microgrid with distributed generators," IET Gener. Transm. Distrib., vol. 11, no. 2, pp. 540–549, 2017, doi: 10.1049/iet-gtd.2016.1144.

[15] M. Singh, T. Vishnuvardhan, and S. G. Srivani, "Adaptive protection coordination scheme for power networks under penetration of distributed energy resources," IET Gener. Transm. Distrib., vol. 10, no. 15, pp. 3919–3929, 2016, doi: 10.1049/iet-gtd.2016.0614.

[16] O. Núñez-Mata, R. Palma-Behnke, F. Valencia, P. Mendoza-Araya, and G. Jiménez-Estévez, "Adaptive protection system for microgrids based on a robust optimization strategy," Energies, vol. 11, no. 2, p. 308, 2018, doi: 10.3390/en11020308.

[17] S. P. George and S. Ashok, “Adaptive differential protection for transformers in grid-connected wind farms,” Int. Trans. Electr. Energy Syst., vol. 28, no. 9, p. e2594, 2018, https://doi.org/10.1002/etep.2594.

[18] E. C. Piesciorovsky and M. F. Ferrari Maglia, “Comparison of high-speed adaptive and nonadaptive backup overcurrent protection on fuse feeders with sensors,” Int. Trans. Electr. Energy Syst., vol. 29, no. 4, p. e2812, 2019, https://doi.org/10.1002/etep.2812.

[19] H. L. R. van der Walt, R. Bansal, and R. Naidoo, “Maintaining overcurrent protection in a PV-based distributed generation power systems,” Int. Trans. Electr. Energy Syst., vol. 28, no. 7, p. e2562, 2018, https://doi.org/10.1002/etep.2562.

[20] A. Alvarez de Sotomayor et al., “IEC 61850-based adaptive protection system for the MV distribution smart grid,” Sustain. Energy, Grids Networks, vol. 15, pp. 26–33, 2018, doi: 10.1016/j.segan.2017.09.003, https://doi.org/10.1016/j.segan.2017.09.003.

[21] O. Anaya-Lara, D. Campos-Gaona, E. Moreno-Goytia, and G. Adam, Offshore wind energy generation: control, protection, and integration to electrical systems. John Wiley & Sons, 2014.

[22] N. W. Miller, W. W. Price, and J. J. Sanchez-Gasca, “Dynamic modeling of GE 1.5 and 3.6 wind turbine-generators,” GE-Power Syst. Energy Consult., vol. 3, no. 3.0, pp. 1977–1983, 2003, https://doi.org/10.1109/PES.2003.1267470.

[23] G. Vahan, S. Booth, V. Gevorgian, and S. Booth, “Review of PREPA technical requirements for interconnecting wind and solar generation,” National Renewable Energy Lab.(NREL), Golden, CO (United States), 2013.Online].Available: https://www.nrel.gov/docs/fy14osti/57089.pdf.

[24] S. Hu, X. Zou, and Y. Kang, “A novel optimal design of DFIG crowbar resistor during grid faults,” in 2014 International Power Electronics Conference (IPEC-Hiroshima 2014-ECCE ASIA), 2014, pp. 555–559, doi: 10.1109/IPEC.2014.6869639.

[25] J. John Justo and K.-S. S. Ro, “Control strategies of doubly fed induction generator-based wind turbine system with new rotor current protection topology,” J. Renew. Sustain. Energy, vol. 4, no. 4, p. 43123, 2012, doi: 10.1063/1.4748808.

[26] T. S. Sidhu and D. Bejmert, “Short-circuit current contribution from large scale PV power plant in the context of distribution power system protection performance,” IET Conf. Publ., vol. 2011, no. 579 CP, p. 134, 2011, doi: 10.1049/cp.2011.0153.

[27] Nematirad R, Pahwa A, Natarajan B, Wu H. Optimal sizing of photovoltaic-battery system for peak demand reduction using statistical models. Frontiers in Energy Research. 2023 Dec 7;11:1297356, DOI:10.3389/fenrg.2023.1297356.

[28] A. H. A. A. Bakar, H. Mokhlis, H. A. Illias, and P. L. Chong, “The study of directional overcurrent relay and directional earth-fault protection application for 33 kV underground cable system in Malaysia,” Int. J. Electr. Power Energy Syst., vol. 40, no. 1, pp. 113–119, 2012, doi: 10.1016/j.ijepes.2012.02.011.

[29] “Real time wind & weather report Parafield Airport - Windfinder.” https://www.windfinder.com/report/parafield_airport (accessed Oct. 24, 2021).

[30] “Past Weather in Adelaide, South Australia, Australia — Yesterday or Further Back.” https://www.timeanddate.com/weather/australia/adelaide/historic (accessed Oct. 24, 2021).

[31] “About the oneminute solar data product - Bureau of Meteorology.” http://www.bom.gov.au/climate/data/oneminsolar/about IDCJAC0022.shtml (accessed Oct. 24, 2021).

[32] Soleymani, S., Talebi, A.: Forecasting solar irradiance with geographical considerations: integrating feature selection and learning algorithms. Asian J. Soc. Sci. Manag. Technol. 6(1), 85–93 (2024), https://www.ajssmt.com/wp6-1.html.

[33] Talebi, A., Haeri Boroujeni, S.P. & Razi, A. Integrating random regret minimization-based discrete choice models with mixed integer linear programming for revenue optimization. Iran J Comput Sci (2024). https://doi.org/10.1007/s42044-024-00193-w.

[34] Nikita Gusarov, Amirreza Talebijamalabad, Iragaël Joly. Exploration of model performances in the presence of heterogeneous preferences and random effects utilities awareness. 2020, https://hal.science/hal-03019739/document.

INFO
Corresponding Author: Amin Dindar, Electric Power Engineers/ Austin, TX, USA.

How to cite/reference this article: Amin Dindar, Adaptive Overcurrent Communication-Based Protection Scheme in Smart Distribution Systems in the Hybrid Grids, *Asian. Jour. Social. Scie. Mgmt. Tech*. 2024; 6(4): 144-158.